JOURNAL OF GEOPHYSICAL RESEARCH, VOL. 115, A04207, doi:10.1029/2009JA014235, 2010

Click Here for Full Article

A three-dimensional asymmetric magnetopause model

R. L. Lin,[1,2] X. X. Zhang,[3] S. Q. Liu,[1] Y. L. Wang,[4] and J. C. Gong[1]

Received 12 March 2009; revised 10 October 2009; accepted 30 October 2009; published 10 April 2010.

[1] A new three-dimensional asymmetric magnetopause model has been developed for corrected GSM coordinates and parameterized by the solar wind dynamic and magnetic pressures ($P_d + P_m$), the interplanetary magnetic field (IMF) B_z, and the dipole tilt angle. On the basis of the magnetopause crossings from Geotail, IMP 8, Interball, TC1, Time History of Events and Macroscale Interactions during Substorms (THEMIS), Wind, Cluster, Polar, Los Alamos National Laboratory (LANL), GOES, and Hawkeye, and the corresponding upstream solar wind parameters from ACE, Wind, or OMNI, this model is constructed by the Levenberg-Marquardt method for nonlinear multiparameter fitting step-by-step over the divided regions. The asymmetries of the magnetopause and the indentations near the cusps are appropriately described in this new model. In addition, the saturation effect of IMF B_z on the subsolar distance and the extrapolation for the distant tail magnetopause are also considered. On the basis of this model, the power law index for the subsolar distance versus $P_d + P_m$ is a bit less than $-1/6$, the northward IMF B_z almost does not influence the magnetopause, and the dipole tilt angle is very important to the north–south asymmetry and the location of indentations. In comparison with the previous empirical magnetopause models based on our database, the new model improves prediction capability to describe the three-dimensional structure of the magnetopause. It is shown that this new model can be used to quantitatively study how $P_d + P_m$ compresses the magnetopause, how the southward IMF B_z erodes the magnetopause, and how the dipole tilt angle influences the north–south asymmetry and the indentations.

Citation: Lin, R. L., X. X. Zhang, S. Q. Liu, Y. L. Wang, and J. C. Gong (2010), A three-dimensional asymmetric magnetopause model, *J. Geophys. Res.*, *115*, A04207, doi:10.1029/2009JA014235.

1. Introduction

[2] The Earth's magnetopause is the result of the interaction between the supersonic solar wind and the Earth's magnetic field. The magnetopause basically separates the interplanetary magnetic field from the Earth's magnetic field and prevents most solar wind plasma from entering the Earth's magnetosphere. It adjoins the low-latitude boundary layer, the entry layer, the cusp, and the plasma mantle [*Eastman et al.*, 2000; *Phan et al.*, 1997]. It is also the place where the reconnection occurs with the mass, energy, and momentum transfer from the magnetosheath into the magnetosphere. Previous theoretical and statistical studies indicate that the global structure of the magnetopause is greatly influenced by the solar wind plasma and the interplanetary magnetic field. Under various solar wind conditions, the magnetopause subsolar distance r_0 can be changed from 5.2 to 14 R_E [*Kuznetsov and Suvorova*, 1998]. When r_0 is less than 6.6 R_E, geosynchronous satellites may cross the magnetopause and experience anomalies such as attitude and angular momentum control distortion [*Shue et al.*, 2001]. Therefore, the prediction of the magnetopause size and shape is important not only for theoretical research and numerical simulation but also for space weather applications.

[3] Various empirical magnetopause models have been developed in the past [*Fairfield*, 1971; *Howe and Binsack*, 1972; *Holzer and Slavin*, 1978; *Formisano et al.*, 1979; *Petrinec et al.*, 1991; *Sibeck et al.*, 1991; *Roelof and Sibeck*, 1993; *Petrinec and Russell*, 1993, 1996; *Kuznetsov and Suvorova*, 1996, 1998; *Shue et al.*, 1997, 1998; *Kawano et al.*, 1999; *Boardsen et al.*, 2000; *Kalegaev and Lyutov*, 2000; *Chao et al.*, 2002]. Most of them were developed mainly on the basis of low-latitude magnetopause crossings with the rotationally symmetric assumption and parameterized by the solar wind dynamic pressure P_d and/or the interplanetary magnetic field (IMF) B_z. These rotationally symmetric models often use an elliptic function, a parabolic function, or the Shue model function as a basic functional form to describe the magnetopause. In order to overcome the limit of an elliptic function, which must cross at some point on the nightside and cannot represent the distant tail magnetopause [*Slavin et al.*, 1985], *Petrinec and Russell* [1996] used the inverse trigonometric functions to describe the nightside magnetopause, and *Kawano et al.* [1999] used

[1]Center for Space Science and Applied Research, Chinese Academy of Sciences, Beijing, China.
[2]Graduate University of Chinese Academy of Sciences, Beijing, China.
[3]National Center for Space Weather, China Meteorological Administration, Beijing, China.
[4]NASA Goddard Space Flight Center, Greenbelt, Maryland, USA.

Copyright 2010 by the American Geophysical Union.
0148-0227/10/2009JA014235

Table 1. Summary of 1226 Magnetopause Crossings

	Solar Wind–Crossing Satellites										
	Cluster	Geotail	GOES	IMP 8	Interball	LANL	Polar	TC1	THEMIS	Wind	Total
ACE	292	119	8	1	31	11	135	246	199	3	1045
Wind	0	125	0	5	51	0	0	0	0	0	181
Total	292	244	8	6	82	11	135	246	199	3	1226

a cylinder to represent the tail magnetopause from the position where its transverse radius ($R = \sqrt{Y^2 + Z^2}$) reaches the maximum. The Shue model function has the flexibility to produce an open or closed magnetopause and has a reasonable extrapolation ability to predict the distant tail magnetopause. In addition, the saturation influence of southward IMF B_z on r_0 is also considered in the *Shue et al.* [1998] model and the *Kuznetsov and Suvorova* [1998] model. It is noted that the *Petrinec and Russell* [1996] model, the *Shue et al.* [1998] model, and the *Chao et al.* [2002] model have an appropriate capability to forecast geosynchronous satellites crossing the magnetopause under extreme solar wind conditions [*Yang et al.*, 2002].

[4] For the high-latitude region, *Formisano et al.* [1979] constructed an average magnetopause size and shape in SM coordinates for two dipole tilt angle (ϕ) values. *Boardsen et al.* [2000] developed a quantitatively empirical high-latitude magnetopause model parameterized by P_d, IMF B_z, and ϕ for corrected GSM coordinates on the basis of the Northern Hemisphere magnetopause crossings. *Boardsen et al.* [2000] did not fully model the three-dimensional magnetopause indentation owing to the limitation of model functions. This model is only valid near the subsolar region and at high latitudes in the near-Earth region with $X_{GSM} \geq -5\ R_E$ and is not appropriate for the low latitudes away from the subsolar region.

[5] Obviously, these available magnetopause models are not satisfactory for describing the global magnetopause structure. The main purpose of this paper is to develop a new three-dimensional global magnetopause model to overcome the limitations and disadvantages of the models mentioned above. In section 2 we collect the available magnetopause crossings from multiple satellites using a more accurate method for the calculation of the solar wind propagating time from upstream satellites to magnetopause crossings to replace the uniform propagating method [*Boardsen et al.*, 2000; *Chao et al.*, 2002] and the constant shift time method [*Shue et al.*, 1997, 1998]. In section 3 we expand the Shue model function to a new function, which can describe the global magnetopause, including the asymmetries and the indentations. On the basis of these data and the new model function, in section 4 we select the parameters important for controlling the size and the shape of the magnetopause by the decrease of the standard deviation, and we get the relationships between them and the magnetopause by the nonlinear multiparameter fitting step-by-step. Additionally, we introduce a new continuous function for the relationship between IMF B_z and the magnetopause to replace a piecewise linear function. In section 5 we briefly discuss the characteristics of this new magnetopause model, including the comparison with previous models on the basis of our data, the influences of P_d and IMF B_z on the magnetopause, and the properties of asymmetry and indentation of magnetopause. The conclusions of the new magnetopause model are given in section 6.

2. Data

[6] In this investigation we collect 1226 magnetopause crossings from Cluster, Geotail, GOES, IMP 8, Interball, Los Alamos National Laboratory (LANL), Polar, TC1, Time History of Events and Macroscale Interactions during Substorms (THEMIS), and Wind with their corresponding 5 min average solar wind parameters from ACE or Wind, including the in situ density ratio of helium to hydrogen (http://www.cddc-dsp.ac.cn/ and ftp://cdaweb.gsfc.nasa.gov/pub/istp/). These magnetopause crossings occur within the period from December 1994 to January 2008. Their summary is listed in Table 1. We also use 1482 online Hawkeye magnetopause crossings with hourly solar wind parameters from OMNI data, including the constant density ratio (0.05) of helium to hydrogen (ftp://nssdcftp.gsfc.nasa.gov/spacecraftdata/magnetopausecrossings). All the data have been transformed from GSM coordinates to corrected GSM (cGSM) coordinates by equations (1) and (2) of *Boardsen et al.* [2000] in order to remove the aberration due to the Earth revolution around the Sun and the wind sock effect due to the solar wind velocity off the Sun-Earth line. We assume the Earth revolution velocity to be 30 km/s in the negative Y_{GSE} direction. Note that only 80% of randomly selected non-Hawkeye crossings (980) are used for modeling, the other 20% of non-Hawkeye crossings (246) are for comparison, all Hawkeye crossings are used only for the indentations' fitting, and all calculations throughout the rest of this paper are performed in cGSM coordinates.

[7] For the low- and middle-latitude magnetopause crossings, we identify them by the sudden change in the strength or the direction of the magnetic field and/or in the plasma parameters [*Shue et al.*, 1997]. For the high-latitude magnetopause crossings, the plasma wave data are also considered to identify magnetopause crossings in order to distinguish the magnetopause from the magnetosheath, the cusp, the entry layer, and the mantle [*Eastman et al.*, 2000]. In non-Hawkeye magnetopause crossings, we have excluded those without a clear identification. The shift time from ACE or Wind to the magnetopause crossings is mainly determined by matching the clock angle of the IMF or the interplanetary plasma parameter (e.g., proton number density) variable profile with that of the magnetosheath. After getting the shift time, we can obtain the corresponding upstream solar wind parameters from ACE or Wind. If these parameters are not complete or not relatively stable within 5 min around the upstream corresponding time, we also exclude them.

[8] If we cannot match the clock angles or the plasma parameter variable profiles between the interplanetary space

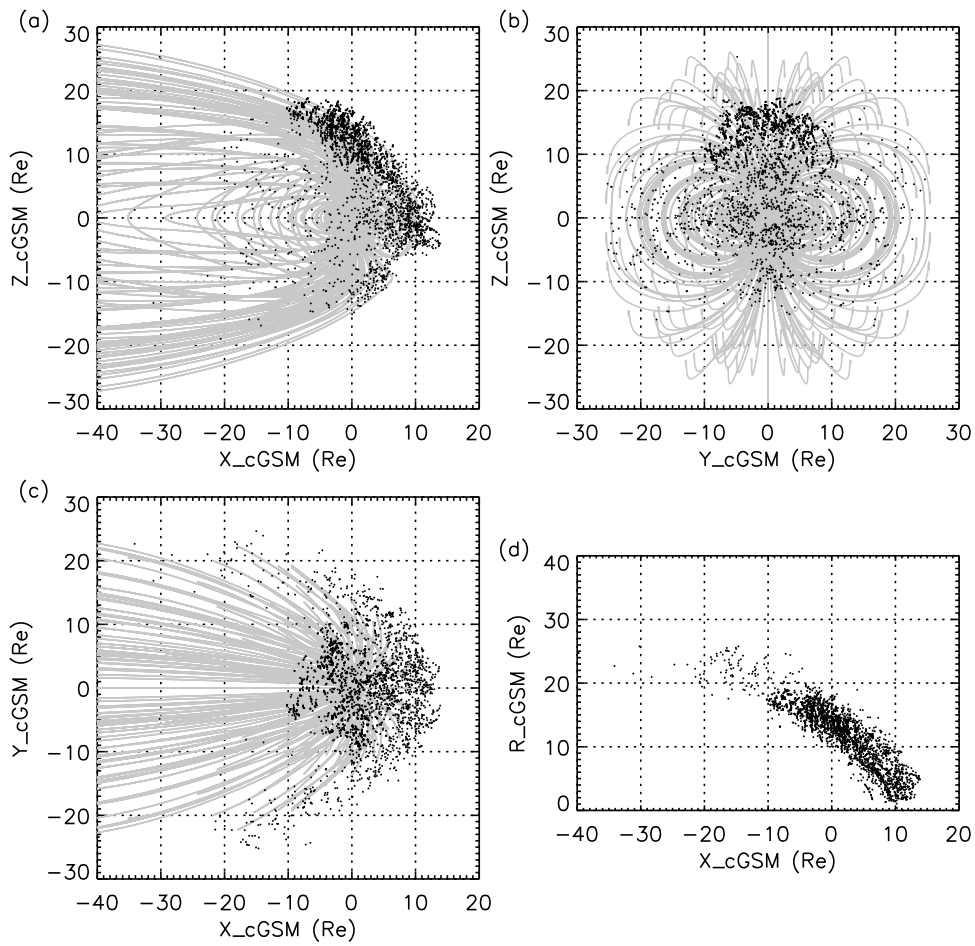

Figure 1. Projections of 2708 magnetopause crossings in the cGSM (a) *X-Z* plane, (b) *Y-Z* plane, (c) *X-Y* plane, and (d) *X-R* plane, where $R_{cGSM} = \sqrt{Y_{cGSM}^2 + Z_{cGSM}^2}$. The dots and the gray curves are the projections of magnetopause crossings and the magnetic field lines from the *Tsyganenko* [1996] magnetic field model, respectively.

and the magnetosheath, we calculate the shift time with the help of a near-Earth satellite (assistant satellite) outside the bow shock during a magnetopause crossing to reduce the deviation of solar wind propagating time. Then the shift time (t_r) from ACE or Wind to the magnetopause-crossing satellite can be obtained by

$$t_r = t_v + \left(t_r' - t_v'\right), \tag{1}$$

where t_v and t'_v are the virtual propagating time from ACE or Wind to the magnetopause-crossing satellite and the assistant satellite by the uniform propagating method, respectively, and t'_r is the assistant shift time given by matching the plasma and IMF parameters from the assistant satellite with those from ACE or Wind. This method can compensate for the deviation of the propagating time calculated by the uniform propagating method. It is good when the assistant satellite is not far away from the magnetopause-crossing satellite.

[9] Figure 1 shows the distribution of 2708 magnetopause crossings in the near-Earth space. It is shown that these crossings mainly distribute in the range with $X_{cGSM} \geq -10\ R_E$, relatively even on both duskside and dawnside and mainly in the Northern Hemisphere for the high-latitude magnetopause crossings. Figure 1d shows that the size of the magnetopause can change in a wide range, with the subsolar distance from 6 to 14 R_E and the terminator distance r_f from 10 to 19 R_E.

[10] Figure 2 shows the histograms of the upstream solar wind parameters and the corrected dipole tilt angle ϕ corresponding to the 2708 magnetopause crossings in this study. Each histogram presents the average value, the minimal value, the maximal value, and the bin size of the parameter. It can be seen that solar wind conditions are widely distributed in large ranges, that most crossings occur under normal solar wind conditions, and that some crossings occur under weak or extreme solar wind conditions.

[11] In Figure 2a, P_d includes the contribution from He^{2+}. We take the in situ density ratio of helium to hydrogen to replace a constant value of 0.05, except for Hawkeye crossings, owing to the lack of observation. On the basis of the observation, the density ratio of helium to hydrogen in solar wind may be highly dynamic. For example, on 28 and 29 May 2001, the density ratio of helium to hydrogen observed by ACE is in the range from 0.003 to 0.252, although

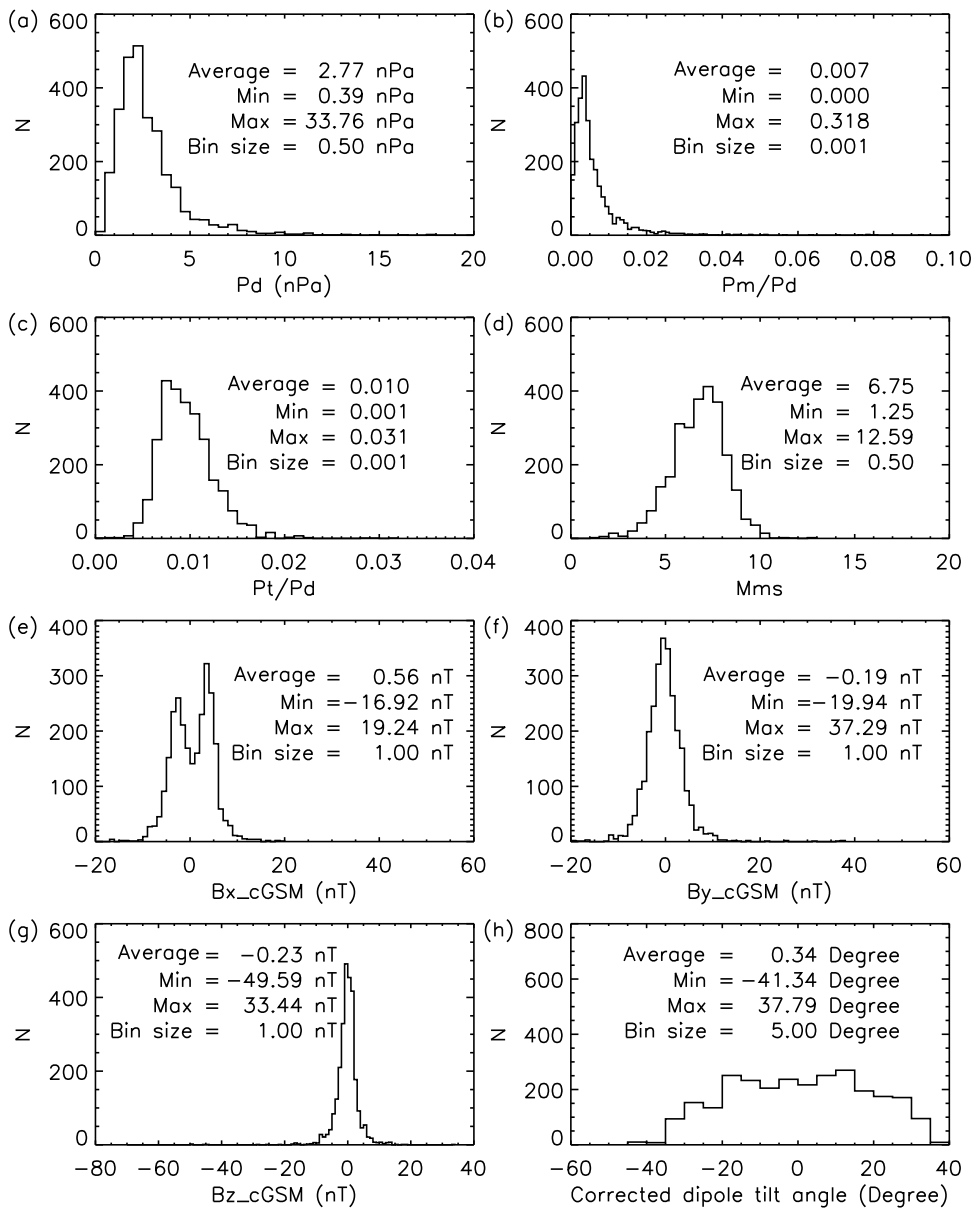

Figure 2. Histograms of the parameters corresponding to the 2708 magnetopause crossings: (a) solar wind dynamic pressure, (b) ratio of solar wind magnetic pressure to dynamic pressure, (c) ratio of solar wind thermal pressure to dynamic pressure, (d) solar wind magnetosonic Mach number, (e) IMF B_{x_cGSM}, (f) IMF B_{y_cGSM}, (g) IMF B_{z_cGSM}, and (h) corrected dipole tilt angle.

the average density ratio is only ~0.061. If it reaches 0.25, the contribution to the solar wind dynamic pressure from He^{2+} is equal to that from H^{+}. In Figure 2b, there are 13 magnetopause crossings with the ratio of solar wind magnetic pressure (P_m) to P_d over 0.1, although the average value of P_m/P_d is only ~0.007. In Figure 2c the ratio of solar wind thermal pressure (P_t) to P_d is less than 0.032 for all magnetopause crossings with the average value of ~0.01. Since the solar wind pressure is one of most important parameters controlling the magnetopause, it is better to use the in situ density ratio of helium to hydrogen and consider the solar wind magnetic pressure in modeling the magnetopause.

[12] As discussed by *Shue et al.* [2000], when a satellite is near its apogee and moving radially most slowly or at geosynchronous orbit at a fixed radial distance, the satellite may have an orbit bias. These crossings usually correspond to extreme solar wind conditions. In order to develop a magnetopause model, which can provide a reasonable magnetopause prediction under extreme solar wind conditions, we keep these crossings for modeling.

3. Construction of the Magnetopause Model Function

[13] It is mentioned in section 1 that the Shue model function is better than other model functions and has the

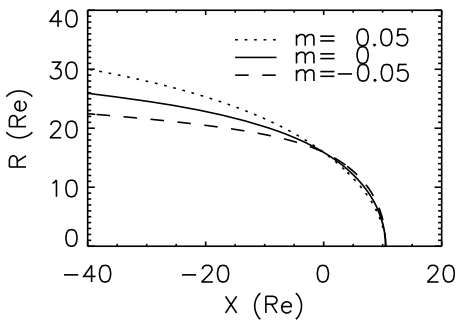

Figure 3. Graphical representation of equation (3) for different m values with r_0 = 10.5 and β = −1.2, where $R = \sqrt{Y^2 + Z^2}$.

flexibility to produce an open or closed magnetopause. This function can describe different magnetopause size and shape by changing the level of the tail flaring (α):

$$r = r_0 \left(\frac{2}{1 + \cos\theta} \right)^{\alpha}, \tag{2}$$

where r is the radial distance at a zenith angle (θ) between the direction of r and the positive X direction. When $\alpha > 0.5$, the magnetopause always flares, and equation (2) represents an open magnetopause. When $0 < \alpha < 0.5$, the magnetopause first flares and then shrinks on the nightside, and equation (2) represents a closed magnetopause [*Shue et al.*, 1997].

[14] According to equation (2), if we fix r_0 and the terminator distance ($r_f = r_0 \cdot 2^{\alpha}$), the whole magnetopause shape will be fixed. It may not be very satisfactory, especially for the tail magnetopause. In order to get a more flexible function for the magnetopause shape, we expand equation (2) as

$$r = r_0 \cdot \left\{ \cos\frac{\theta}{2} + m \cdot \sin(2\theta) \cdot [1 - \exp(-\theta)] \right\}^{\beta}, \tag{3}$$

where β controls the level of the tail flaring, m adjusts the magnetopause shape without influencing r_0 and r_f, and $1 - \exp(-\theta)$ keeps the magnetopause shape smooth near the subsolar point. When m = 0, equation (3) becomes equation (2) ($\beta = -2\alpha$). As shown in Figure 3, when $m > 0$, the magnetopause moves inward on the dayside and outward on the nightside, and vice versa when $m < 0$.

[15] Considering the asymmetries and the indentations of magnetopause, we introduce an azimuth angle (φ), the angle between the projection of r in the Y-Z plane and the direction of the positive Y axis from 0 and 2π in clockwise looking from the Earth to the Sun, and equation (3) is rewritten as

$$r = r_0 \cdot \left\{ \cos\frac{\theta}{2} + m \cdot \sin(2\theta) \cdot [1 - \exp(-\theta)] \right\}^{\beta} + Q, \tag{4}$$

where

$$\beta = \beta_0 + \beta_1 \cdot \cos\varphi + \beta_2 \cdot \sin\varphi + \beta_3 \cdot (\sin\varphi)^2, \tag{5}$$

$$Q = c_n \cdot \exp\left(d_n \cdot \psi_n^{e_n}\right) + c_s \cdot \exp\left(d_s \cdot \psi_s^{e_s}\right), \tag{6}$$

$$\psi_n = \arccos[\cos\theta \cdot \cos\theta_n + \sin\theta \cdot \sin\theta_n \cdot \cos(\varphi - \varphi_n)], \tag{7}$$

$$\psi_s = \arccos[\cos\theta \cdot \cos\theta_s + \sin\theta \cdot \sin\theta_s \cdot \cos(\varphi - \varphi_s)], \tag{8}$$

where β_0 controls the tail flaring of the rotationally symmetric magnetopause; $\beta_1 \cdot \cos\varphi$, $\beta_2 \cdot \sin\varphi$, $\beta_3 \cdot (\sin\varphi)^2$, $c_n \cdot \exp(d_n \cdot \psi_n^{e_n})$, and $c_s \cdot \exp(d_s \cdot \psi_s^{e_s})$ describe the asymmetry along the Y direction, the asymmetry along the Z direction, the difference between the transverse diameter of the tail magnetopause along the Y direction and that along the Z direction, and the north and the south indentations, respectively; β_1 and β_2 control the extent of the asymmetries; β_3 controls the eccentricity of the subelliptical shape of tail magnetopause transverse cross section; c_n (c_s), d_n (d_s), and e_n (e_s) control the depth, the scope, and the shape of the north (the south) indentation; θ_n (θ_s) and φ_n (φ_s) are the zenith angle and the azimuth angle of the north (the south) indentation vertex, respectively; and ψ_n or ψ_s is the angle between the direction of r and the direction from the Earth to the north or the south indentation vertex from 0 to π. All angles are in radian in equations (4)–(8). According to the physical significance of r_0, β_0, β_1, β_2, β_3, and Q, we can fit them step-by-step by the divided-region method.

[16] In order to demonstrate that equation (4) can be appropriate for describing the global structure of magnetopause, including the asymmetries and the indentations, we let r_0 = 10.8, m = 0.1, β_0 = −1.03, β_1 = −0.07, β_2 = −0.02, β_3 = 0.09, c_n = −6, d_n = −10, e_n = 1, c_s = −7, d_s = −6, e_s = 1, θ_n = 0.64, $\varphi_n = \frac{\pi}{2}$, θ_s = 1.25, and $\varphi_s = \frac{3\pi}{2}$ for equation (4), and we let P_d = 2 nPa, D_{ST} = 0 nT, B_y = 0 nT, and B_z = 0 nT for the *Tsyganenko* [1996] magnetic field model when ϕ = 20°. As shown in Figure 4a, the magnetopause (black curve) from equation (4) coincides with the outermost magnetic field lines (gray curves) from the *Tsyganenko* [1996] magnetic field model very well under the above condition. Figure 4b further demonstrates that equation (4) can also describe a three-dimensional magnetopause shape well, including the asymmetries and the indentations. Equation (4) will be used to fit the magnetopause crossings in section 4.

4. Three-Dimensional Asymmetric Magnetopause Model Fitting

[17] On the basis of the magnetopause crossings' data in section 2 and the magnetopause model function in section 3, a new three-dimensional magnetopause model will be developed by the Levenberg-Marquardt method for nonlinear multiparameter fitting [*Press et al.*, 1992] step-by-step for different parameters: r_0, β_0, β_1, β_2, β_3, and Q. This method can effectively separate the influences of different parameters on the same region and the influences of the same parameter on different regions. During fitting of the magnetopause crossings, the decrease of the standard deviation

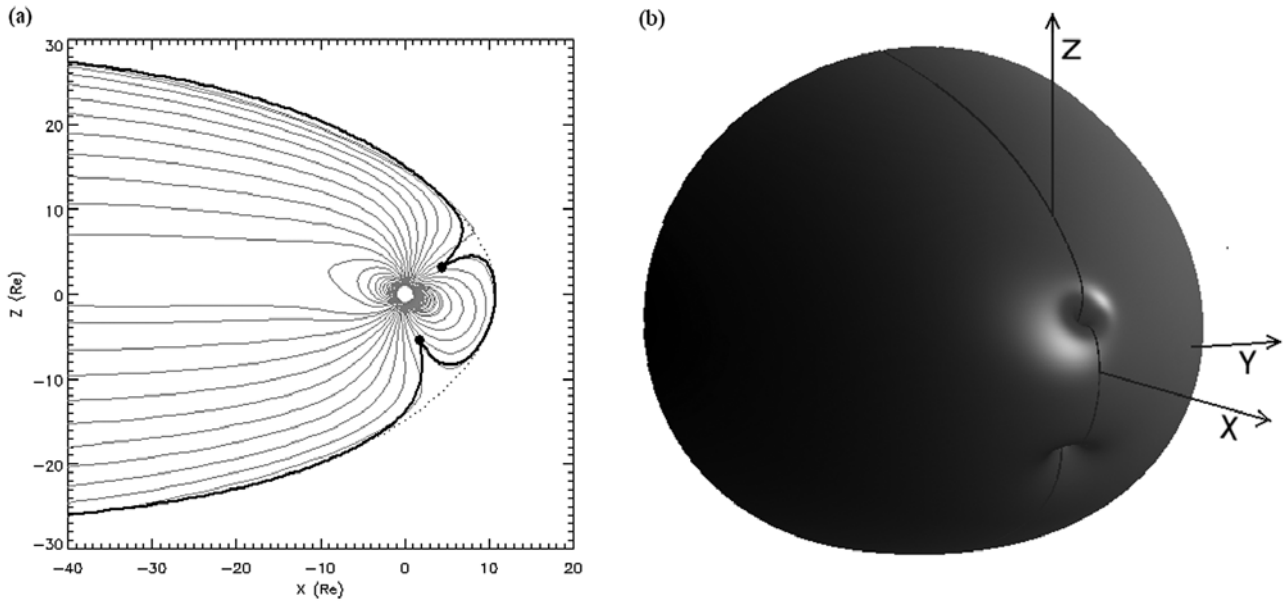

Figure 4. Graphical representation of the magnetopause from equation (4). (a) The black curve is the magnetopause shape from equation (4), the gray curves are the magnetic field lines from the *Tsyganenko* [1996] magnetic field model in the *X*-*Z* plane, the dotted curve is the magnetopause from equation (4) without considering the indentations, and both black dots are the vertexes of indentations. (b) The surface of a three-dimensional magnetopause from equation (4).

(σ) will be used to determine the important parameters that control the coefficients in equation (4).

4.1. The r_0 Fitting

[18] As shown in Figure 1, there are not too many crossings near the subsolar point. For r_0 fitting, the crossings around the subsolar point within a cutoff value θ_c can be used after normalization. On the basis of the *Shue et al.* [1998] model, α can change from 0.510 to 0.686 for 1 nPa $\leq P_d \leq$ 10 nPa and −10 nT $\leq B_z \leq$ 10 nT, so the normalized r_0 will be calculated by equation (2) with α = 0.6 first. After taking into account the deviation of the normalized r_0 and the location of magnetopause indentations, we choose θ_c = 30°. This leads to 247 magnetopause crossings for r_0 fitting and only introduces the absolute value of the relative deviation less than 2% for $0.35 \leq \alpha \leq 0.85$ according to equation (2).

[19] On the basis of the relationship between P_d and r_0 [e.g., *Spreiter et al.*, 1966], the statistical results of the IMF B_z influence on r_0 [e.g., *Shue et al.*, 1998], and the consideration of the saturation influence of the southward IMF B_z on r_0 [*Yang et al.*, 2003], we start the fitting equation with

$$r_0 = \mathrm{a}_0 \cdot (P_d + P_m)^{\mathrm{a}_1} \cdot \left[1 + \mathrm{a}_2 \cdot \frac{\exp(\mathrm{a}_3 \cdot B_z) - 1}{\exp(\mathrm{a}_4 \cdot B_z) + 1}\right]. \quad (9)$$

The fitting values of the coefficients for equation (9) are listed in Table 2.

Table 2. Values of Coefficients From Equation (9) Fitting

a_0	a_1	a_2	a_3	a_4	$\sigma(r_0)$
12.122	−0.190	0.282	0.068	2.241	0.611

[20] In order to investigate whether other parameters are also important to r_0, equation (9) is rewritten as

$$r_0 = \mathrm{a}_0 \cdot (P_d + P_m)^{\mathrm{a}_1} \cdot \left[1 + \mathrm{a}_2 \cdot \frac{\exp(\mathrm{a}_3 \cdot B_z) - 1}{\exp(\mathrm{a}_4 \cdot B_z) + 1}\right] \cdot f(x), \quad (10)$$

where

$$f(x) = 1 + \mathrm{a}_5 \cdot x + \mathrm{a}_6 \cdot x^2 + \mathrm{a}_7 \cdot x^3 + \mathrm{a}_8 \cdot x^4. \quad (11)$$

The x is the parameter that may be important to r_0. Table 3 shows that there is no obvious decrease on $\sigma(r_0)$ after we take into account the influences of other parameters, including the magnetosonic Mach number (M_{MS}). Therefore, we only consider the influences of $P_d + P_m$ and IMF B_z on r_0. Note that in the tail flaring and indentations' fittings in sections 4.2–4.4, the coefficients' values listed in Table 2 for r_0 are fixed in order to separate the influences of $P_d + P_m$ and IMF B_z on the subsolar distance from their influences on the other regions.

4.2. The β_0 and β_1 Fitting

[21] According to equation (4), the influences of $\beta_2 \cdot \sin \varphi$, $\beta_3 \cdot (\sin \varphi)^2$, and Q on the low-latitude magnetopause can be ignored temporarily. This leads to 422 magnetopause crossings with $|Z| \leq 3\ R_E$ for β_0 and β_1 fitting.

[22] On the basis of previous magnetopause models, the low-latitude magnetopause can be thought to be symmetric

Table 3. The $\sigma(r_0)$ From Equation (10) Fitting With Different Parameters

x	0	B_x	B_y	ϕ	P_t	P_m	M_{MS}
$\sigma(r_0)$	0.611	0.603	0.597	0.593	0.608	0.595	0.591

Table 4. The $\sigma(r)$ From Equation (12) Fitting With Different Parameters

x	0	B_x	B_y	B_z	ϕ	P_d	P_m	P_t	M_{MS}
$\sigma(r)$	0.871	0.829	0.816	0.783	0.861	0.867	0.861	0.861	0.848

along the Y direction by the first-order approximation, so the fitting equation for r is started with

$$r = r_0 \cdot \left\{ \cos\frac{\theta}{2} + \mathrm{a}_5 \cdot \sin(2\theta) \cdot [1 - \exp(-\theta)] \right\}^{\beta_0(x)}, \qquad (12)$$

where

$$\beta_0(x) = \mathrm{a}_6 + \mathrm{a}_7 \cdot x + \mathrm{a}_8 \cdot x^2 + \mathrm{a}_9 \cdot x^3 + \mathrm{a}_{10} \cdot x^4. \qquad (13)$$

The r_0 is calculated by equation (9) with the coefficients listed in Table 2, and x is the parameter that may be important to β_0. According to the fitting results listed in Table 4, IMF B_z is chosen as the most important parameter to the tail flaring owing to its contribution to the decrease of $\sigma(r)$. As in section 4.1, the other parameters are ignored for β_0.

[23] Considering the asymmetry along the Y direction, equation (12) is rewritten as

$$r = r_0 \cdot \left\{ \cos\frac{\theta}{2} + \mathrm{a}_5 \cdot \sin(2\theta) \cdot [1 - \exp(-\theta)] \right\}^{\beta_0(B_Z) + \beta_1(x) \cdot \cos\varphi}, \qquad (14)$$

where

$$\beta_1(x) = \mathrm{a}_{11} + \mathrm{a}_{12} \cdot x + \mathrm{a}_{13} \cdot x^2 + \mathrm{a}_{14} \cdot x^3 + \mathrm{a}_{15} \cdot x^4. \qquad (15)$$

The x is the parameter that may be important to β_1. As shown in Table 5, if the intrinsic asymmetry along the Y direction ($\beta_1(0) = \mathrm{a}_{11}$) is considered in equation (14), $\sigma(r)$ can decrease from 0.783 to 0.724 R_E. It is also noted that the other parameters have little effect on the asymmetry along the Y direction; thus we choose $\beta_1 = \mathrm{a}_{11}$.

[24] According to the equation (14) fitting with $\beta_1 = \mathrm{a}_{11}$, the relationship between B_z and β_0 is determined, as the dotted curve shows in Figure 5. In these 422 magnetopause crossings, most of them are in the range of -15 nT $\leq B_z \leq$ 5 nT, and there are only 9 crossings with $B_z < -15$ nT and 11 crossings with $B_z > 5$ nT. Therefore, the dotted curve in Figure 5 in the range of -15 nT $\leq B_z \leq$ 5 nT is reliable. On the basis of this segment of dotted curve and the consideration of the extrapolation for B_z, the equations for β_0 and β_1 fitting are finally defined by

$$\beta_0 = \mathrm{a}_6 + \mathrm{a}_7 \cdot \frac{\exp(\mathrm{a}_8 \cdot B_z) - 1}{\exp(\mathrm{a}_9 \cdot B_z) + 1}, \qquad (16)$$

$$\beta_1 = \mathrm{a}_{10}. \qquad (17)$$

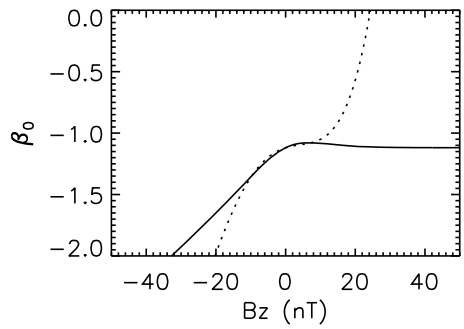

Figure 5. Comparison between the result of $\beta_0(B_Z)$ from the equations (14), (16), and (17) fitting (solid curve) and that from the equations (13)–(15) fitting with $\beta_1 = \mathrm{a}_{11}$ (dotted curve).

[25] As shown in Figure 5, the solid curve from the equation (14), (16), and (17) fitting coincides very well with the dotted curve from the equations (13)–(15) fitting with $\beta_1 = \mathrm{a}_{11}$ in the range of -15 nT $\leq B_z \leq$ 5 nT, and equation (16) overcomes the extrapolation limitation of equation (13). The fitting coefficients for equation (14), (16), and (17) are listed in Table 6 and only provide initial values for further fitting.

4.3. The β_2 and β_3 Fitting

[26] On the basis of previous studies about the high-latitude magnetopause crossings, the size of the high-latitude magnetopause is smaller than that of the low-latitude magnetopause on the dayside [*Sibeck et al.*, 1991; *Zhou and Russell*, 1997; *Boardsen et al.*, 2000; *Šafránková et al.*, 2002, 2005]. This difference may mainly result from the asymmetries (β_2 and β_3) and the indentations near the north and south cusps (Q).

[27] Let us first consider the influences of β_2 and β_3. (Q is considered in section 4.4.) In order to avoid the influence of indentations, we select 594 magnetopause crossings in the region with $X \leq -5$ R_E or in the region with $|\sin\varphi| \leq \sin 40°$. As in section 4.2, we keep their intrinsic asymmetries and the first-order influence of ϕ on the asymmetry along the Z direction. Therefore, the fitting equation is defined by

$$r = r_0 \cdot \left\{ \cos\frac{\theta}{2} + \mathrm{a}_5 \cdot \sin(2\theta) \cdot [1 - \exp(-\theta)] \right\}^{\beta}, \qquad (18)$$

where β is defined by equation (5), β_0 and β_1 are defined by equations (16) and (17), $\beta_2 = \mathrm{a}_{11} + \mathrm{a}_{12} \cdot \phi$, and $\beta_3 = \mathrm{a}_{13}$. The fitting coefficients for equation (18) are listed in Table 7. As in section 4.2, when we fit equation (18), the coefficients listed in Table 2 for r_0 are fixed and the coefficients listed in Table 6 only provide the initial values for the equation (18) fitting.

4.4. The Q Fitting

[28] In order to appropriately reproduce the indentations, we add 1482 Hawkeye magnetopause crossings with hourly

Table 5. The $\sigma(r)$ From Equations (13)–(15) Fitting With Different Parameters

		$\beta_1(x) \neq 0$								
x	$\beta_1(x) = 0$, 0	0	B_x	B_y	B_z	ϕ	P_d	P_m	P_t	M_{MS}
$\sigma(r)$	0.783	0.724	0.714	0.712	0.708	0.723	0.722	0.713	0.720	0.703

Table 6. Values of Coefficients From Equations (14), (16), and (17) Fitting

a_5	a_6	a_7	a_8	a_9	a_{10}	$\sigma(r)$
0.0168	−1.119	25.406	0.00108	0.190	0.0574	0.727

solar wind parameters along with 980 non-Hawkeye magnetopause crossings with 5 min average solar wind parameters. For simplicity, we will only consider the influences of $P_d + P_m$ and ϕ on the indentations and assume the following: (1) the north and the south indentation vertexes are in the *Y-Z* plane, and (2) the influences of ϕ on the north and the south indentations are antisymmetric. As in section 4.1, equation (4) is finally defined by

$$r = r_0 \cdot f(\theta, \varphi, \phi) + c_n \cdot \exp\left(d_n \cdot \psi_n^{e_n}\right) + c_s \cdot \exp\left(d_s \cdot \psi_s^{e_s}\right), \quad (19)$$

where

$$\begin{aligned}
r_0 &= a_0 \cdot (P_d + P_m)^{a_1} \cdot \left[1 + a_2 \cdot \frac{\exp(a_3 \cdot B_z) - 1}{\exp(a_4 \cdot B_z) + 1}\right], \\
f(\theta, \varphi, \phi) &= \left\{ \cos\frac{\theta}{2} + a_5 \cdot \sin(2\theta) \cdot [1 - \exp(-\theta)] \right\}^{\beta_0 + \beta_1 \cdot \cos\varphi + \beta_2 \cdot \sin\varphi + \beta_3 \cdot (\sin\varphi)^2}, \\
\beta_0 &= a_6 + a_7 \cdot \frac{\exp(a_8 \cdot B_z) - 1}{\exp(a_9 \cdot B_z) + 1}, \\
\beta_1 &= a_{10}, \\
\beta_2 &= a_{11} + a_{12} \cdot \phi, \\
\beta_2 &= a_{13}, \\
c_n &= c_s = a_{14} \cdot (P_d + P_m)^{a_{15}}, \\
d_n &= a_{16} + a_{17} \cdot \phi + a_{18} \cdot \phi^2, \\
d_s &= a_{16} - a_{17} \cdot \phi + a_{18} \cdot \phi^2, \\
\psi_n &= \arccos\left[\cos\theta \cdot \cos\theta_n + \sin\theta \cdot \sin\theta_n \cdot \cos\left(\varphi - \frac{\pi}{2}\right)\right], \\
\psi_s &= \arccos\left[\cos\theta \cdot \cos\theta_s + \sin\theta \cdot \sin\theta_s \cdot \cos\left(\varphi - \frac{3\pi}{2}\right)\right], \\
\theta_n &= a_{19} + a_{20} \cdot \phi, \\
\theta_s &= a_{19} - a_{20} \cdot \phi, \\
e_n &= e_s = a_{21}.
\end{aligned} \quad (20)$$

[29] When fitting Q, we use the Hawkeye magnetopause crossings with hourly solar wind parameters but not the 5 min average, so all coefficients' values, except the coefficients of Q, are fixed. If these coefficients are not fixed, the low-resolution Hawkeye magnetopause crossings' data will influence the fitting results from the high-resolution data.

Table 8. Initial Values of Coefficients From Equation (19) Fitting

a_{14}	a_{15}	a_{16}	a_{17}	a_{18}	a_{19}	a_{20}	a_{21}	$\sigma(r)$
−4.189	−0.553	−2.607	0.390	−5.392	1.142	−0.882	1.463	1.043

By this method and the Levenberg-Marquardt method for nonlinear multiparameter fitting, the coefficients' values of Q from the equation (19) fitting are determined and listed in Table 8.

4.5. Adjusting the Fitting Coefficients

[30] As mentioned in section 4.1, when we normalize the crossings with $\theta \leq 30°$ for r_0 fitting, we ignore the influence of the solar wind parameters on α and the influence of the indentations on r_0. Now we will consider these influences on the basis of equation (19). The normalized r_0 for the magnetopause crossings with $\theta \leq 30°$ will be calculated by equation (19) with the coefficients listed in Tables 2, 7, and 8, and then equation (9) will be fitted with the initial values of the coefficients listed in Table 2. Since r_0 has been adjusted, we need to fit equations (14), (16), and (17) with the initial values of the coefficients listed in Table 7 and then fit equation (18) as done in section 4.3. Finally, we fit equation (19) with the initial values of the coefficients listed in Table 8. After the fitting processes above, all coefficients for equation (19) are finally determined and listed in Table 9. On the basis of the above fittings, a new three-dimensional asymmetric magnetopause model has finally been constructed and parameterized by the solar wind dynamic and magnetic pressures ($P_d + P_m$), the interplanetary magnetic field (IMF) B_z, and the corrected dipole tilt angle (ϕ).

5. Characteristics of the New Model

5.1. Comparison With Previous Models

[31] In order to better evaluate the new magnetopause model, the standard deviation $\sigma(d)$ is used to compare the new model with the previous models on the basis of 246 independent non-Hawkeye magnetopause crossings with 5 min average solar wind parameters, where d is the minimal distance from the observed magnetopause crossing to the predicted magnetopause surface. Table 10 lists the distribution of $\sigma(d)$ in different regions for the magnetopause models using 246 independent non-Hawkeye magnetopause crossings. It is shown that the *Petrinec and Russell* [1996] model, the *Shue et al.* [1997] model, the *Shue et al.* [1998] model, and the *Chao et al.* [2002] model are appropriate for the low-latitude region ($|Z| \leq 3\ R_E$) with $\sigma(d)$ less than 0.8 R_E, whereas all previous low-latitude magnetopause models for the middle- and high-latitude region ($|Z| > 3\ R_E$) get $\sigma(d)$ more than 1.3 R_E. The last row in Table 10 lists the percentage of the $\sigma(d)$ decrease by comparing the new model with the best previous low-latitude model in each region. Table 10 indicates that the new model has greatly improved prediction capability. Note that when we calculate $\sigma(d)$ for the previous models, the

Table 7. Values of Coefficients From Equation (18) Fitting

a_5	a_6	a_7	a_8	a_9	a_{10}	a_{11}	a_{12}	a_{13}	$\sigma(r)$
0.0248	−1.110	2.481	0.0118	0.366	0.0456	−0.00808	−0.208	0.0402	1.057

Table 9. Final Values of Coefficients From Equation (19) Fitting

Coefficient	Value
a_0	12.544
a_1	−0.194
a_2	0.305
a_3	0.0573
a_4	2.178
a_5	0.0571
a_6	−0.999
a_7	16.473
a_8	0.00152
a_9	0.382
a_{10}	0.0431
a_{11}	−0.00763
a_{12}	−0.210
a_{13}	0.0405
a_{14}	−4.430
a_{15}	−0.636
a_{16}	−2.600
a_{17}	0.832
a_{18}	−5.328
a_{19}	1.103
a_{20}	−0.907
a_{21}	1.450
σ (r)	1.033

data have been converted to their required coordinate systems, and we assume that these models are valid for these data. Table 10 also indicates that $\sigma(d)$ increases with θ for all magnetopause models; that is, the tail magnetopause is less accurately determined than is the nose magnetopause.

[32] For comparison with the *Boardsen et al.* [2000] model, 124 independent non-Hawkeye magnetopause crossings with the magnetic local time between 9 and 15 h and $X \geq -5\ R_E$ are selected. For the magnetopause crossings with the invariant latitude less than 81°, the *Boardsen et al.* [2000] nose model is used; for the other magnetopause crossings, the *Boardsen et al.* [2000] antisunward model and the symmetry assumption 3 from section 4 of *Boardsen et al.* [2000] in the Southern Hemisphere are used. On the basis of these data, $\sigma(d)$ is 0.867 R_E for the *Boardsen et al.* [2000] model and reduced to 0.626 R_E for our new model.

[33] The differences in deviations between these models may come from the following reasons: (1) the model function for the magnetopause shape, (2) the functions for the influence of the IMF B_z on the coefficients of the model function, (3) the control parameters in the model function, (4) the fitting method, (5) the data resolution of the corresponding upstream solar wind parameters, and (6) the method to match the upstream solar wind parameters for the magnetopause crossings.

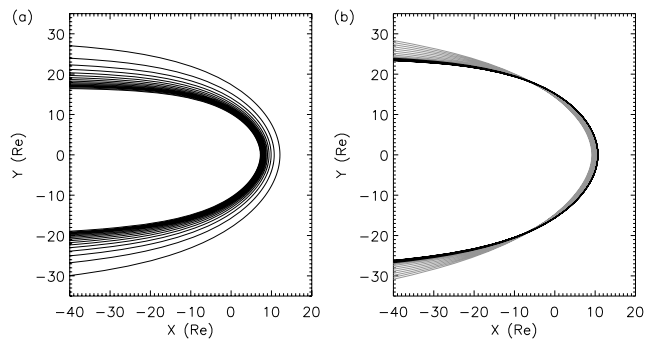

Figure 6. Influences of P_d and IMF B_z on the magnetopause in the X-Y plane: (a) $\phi = 0°$, $|B| = |B_z|$, $B_z = 0$ nT, and P_d increases from 1 to 16 nPa with 1 nPa interval; and (b) $\phi = 0°$, $|B| = |B_z|$, $P_d = 2$ nPa, and B_z increases from −10 to 10 nT with 1 nT interval. The black curves correspond to $B_z \geq 0$ nT, and the gray curves correspond to $B_z < 0$ nT.

5.2. Influences of P_d and IMF B_z on the Magnetopause

[34] Figure 6 shows the influences of P_d and IMF B_z on the magnetopause in the X-Y plane. As shown in Figure 6a, the increasing P_d causes the decrease of the magnetopause size but almost keeps the magnetopause shapes self-similar. On the basis of the new model, the power law index for r_0 versus P_d is −0.194: a bit less than the theoretical prediction, −1/6, for a dipole in a vacuum. As shown in Figure 6b, the increasing southward IMF B_z causes the decrease of r_0 and the increase of the tail flaring. This result indicates that the southward IMF B_z can erode the dayside magnetic flux to the nightside. Figure 6b also shows that the northward IMF B_z almost does not influence the magnetopause. These results indicate that the reconnection between the interplanetary magnetic field and the Earth magnetic filed is strong for the southward IMF B_z but weak for the northward IMF B_z. The IMF B_z influences on the magnetopause subsolar distance and tail flaring are consistent with its influence on the cusp [*Zhou et al.*, 2000].

5.3. Asymmetries

[35] Figure 7 shows the cross sections of magnetopause at different X for different corrected dipole tilt angles. Figure 7 shows the asymmetries of magnetopause along the

Table 10. Distribution of the Standard Deviation $\sigma(d)$ in Different Regions for the 246 Independent Non-Hawkeye Magnetopause Crossings

Model	θ			Z		
	$\theta \leq 30°$ (62)	$30° < \theta < 90°$ (128)	$\theta \geq 90°$ (56)	$\lvert Z\rvert \leq 3\ R_E$ (108)	$\lvert Z\rvert > 3\ R_E$ (138)	All (246)
Roelof and Sibeck [1993]	0.958	1.297	1.957	1.123	1.594	1.407
Petrinec and Russell [1996]	0.703	1.148	1.446	0.739	1.366	1.134
Shue et al. [1997]	0.791	1.179	1.457	0.783	1.397	1.168
Shue et al. [1998]	0.791	1.194	1.479	0.780	1.420	1.182
Kuznetsov and Suvorova [1998]	0.651	1.079	2.297	1.023	1.610	1.383
Kawano et al. [1999]	1.000	1.253	1.583	1.075	1.420	1.280
Kalegaev and Lyutov [2000]	0.924	1.208	3.600	1.133	2.448	1.981
Chao et al. [2002]	0.709	1.178	1.423	0.724	1.387	1.144
New model	0.539	0.716	0.988	0.615	0.840	0.750
$\delta\sigma(d)/\sigma(d)$	17.2%	33.6%	30.6%	15.1%	38.5%	33.9%

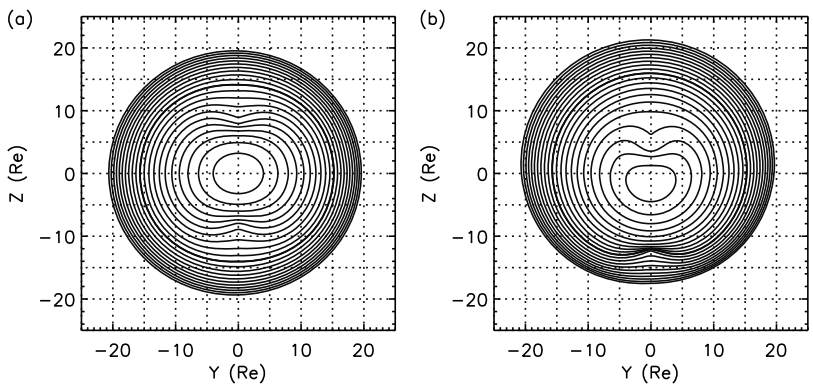

Figure 7. Cross sections of magnetopause at different X from −10 to 10 R_E with 1 R_E interval for P_d = 2 nPa, |B| = 5 nT, and B_z = 0 nT: (a) ϕ = 0° and (b) ϕ = 35°. The thick solid curves are for X = 0 R_E.

Y direction and along the Z direction. As shown in Figure 7a, when ϕ = 0°, the asymmetry along the Y direction or along the Z direction is not obvious, whereas the size of magnetopause along the Z direction is obviously smaller than that along the Y direction in the indentations' region but not obvious in the other regions. Figure 7b is for ϕ = 35°. It is found that the asymmetry along the Z axis becomes more obvious, owing to the swinging of the magnetopause and the displacement of the indentations, but the asymmetry along the Y axis is almost not affected. It is also found that the increase of ϕ displaces the magnetopause outward in the Northern Hemisphere and inward in the Southern Hemisphere, makes the north indentation closer to the subsolar point and the south indentation farther away from the subsolar point, and moves the centers of the cross sections slightly toward the negative Z direction in the subsolar region and toward the positive Z direction in the tail region.

5.4. Indentations

[36] Figure 8 shows the magnetopause shapes from the new model and the magnetic field lines from the *Tsyganenko* [1996] model in the X-Z plane with different ϕ

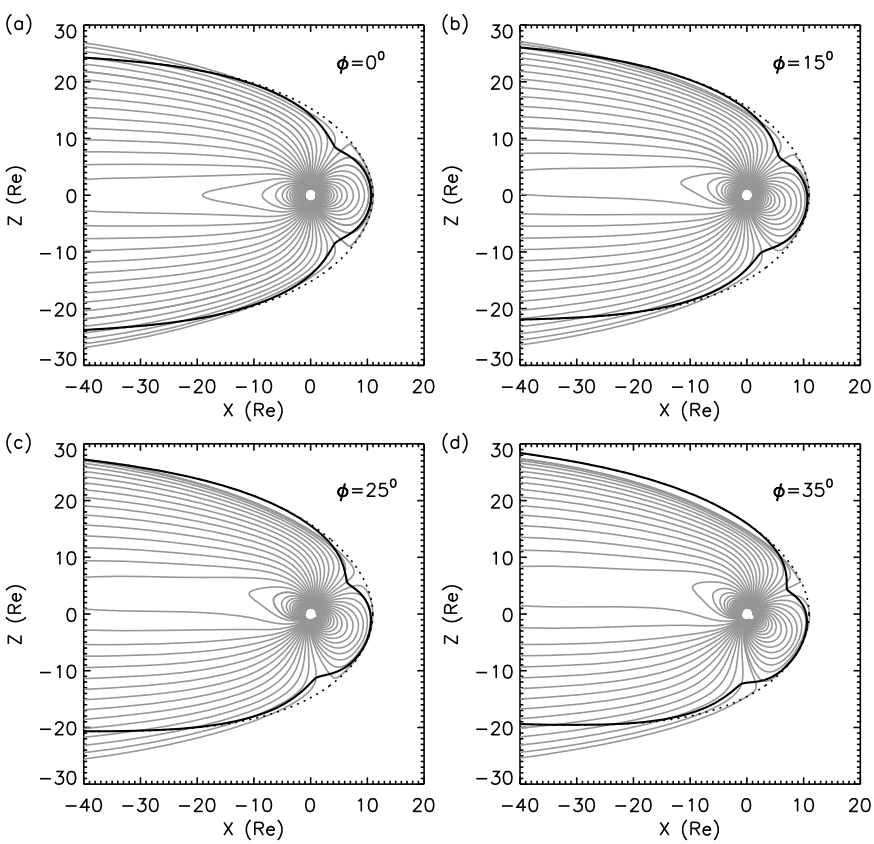

Figure 8. (a–d) Magnetopause shapes (thick solid curves) from the new magnetopause model and the magnetic field lines (gray curves) from the *Tsyganenko* [1996] model with 2° invariant latitude interval in the X-Z plane with different ϕ values. The dotted curves are from the new magnetopause model without considering the indentations.

values for P_d = 2 nPa, $|\vec{B}|$ = 5 nT, B_z = 0 nT, D_{ST} = −10 nT, and B_y = 0 nT. In this case, we take the component of the solar wind velocity V_{y_GSE} = −30 km/s and V_{z_GSE} = 0 km/s, so cGSM coordinates coincide with GSM coordinates.

[37] Figure 8a shows that the depth of the indentation is ~3 R_E from the vertex to the dotted curve, the invariant latitude corresponding to the indentation vertex (ω) is ~80°, and the invariant latitudinal width of the indentation is ~6°, according to the *Tsyganenko* [1996] model. It can be seen that the indentations are near the center of the "funnel" of magnetic field and that ω nearly coincides with the invariant latitude corresponding to the center of the cusp.

[38] Figure 8 demonstrates that the location of the indentations is obviously controlled by ϕ. When ϕ increases from 0° to 35°, the location of the north indentation vertex (θ_n) decreases from 63° to 31°, and the location of the south indentation vertex (θ_s) increases from 63° to 95°, whereas ω_n or ω_s only changes about 1° around 80°. Figure 8 also shows that the depth and the invariant latitudinal width of the indentations do not change much with changing ϕ.

[39] According to the new model, the depth of the indentations is mainly controlled by $P_d + P_m$. The increase of $P_d + P_m$ compresses the whole magnetopause, and the size of the magnetopause decreases; so does the depth of the indentations.

[40] The above conclusions are basically consistent with those from *Šafránková et al.* [2002, 2005]: (1) the dayside magnetopause is indented in the cusp region; (2) an average depth is ~2.5 R_E, but the magnetopause was often observed ~4 R_E below the expected location according to the *Petrinec and Russell* [1996] model; (3) the dimension of the indentation does not depend on the dipole tilt angle, whereas its location does; and (4) the indentation can be observed at geomagnetic latitudes higher than 30° and in a broad range of X_{GSE} coordinates ($-2\ R_E \leq X_{GSE} \leq 8\ R_E$).

[41] *Šafránková et al.* [2002] also concluded that the location and/or extent of the indentation seem to be controlled by the IMF B_z component. However, the new model does not consider the IMF B_z influence in the present investigation. The new model needs more work to explore the influence of the IMF B_z on the indentations of the magnetopause.

6. Conclusions

[42] In this paper a new three-dimensional asymmetric magnetopause model is developed for corrected GSM coordinates and parameterized by the solar wind dynamic and magnetic pressures ($P_d + P_m$), the interplanetary magnetic field (IMF) B_z, and the dipole tilt angle (ϕ) on the basis of 980 magnetopause crossings from Geotail, IMP 8, Interball, TC1, THEMIS, Wind, Cluster, Polar, LANL, and GOES with 5 min average solar wind parameters and 1482 Hawkeye magnetopause crossings with hourly solar wind parameters. The shift time of solar wind propagating from the upstream satellite to the magnetopause crossings is mainly calculated by matching the clock angle of the IMF or the interplanetary plasma parameter variable profile with that of the magnetosheath. The important control parameters for the magnetopause are selected according to the decrease of the standard deviation, and the relationships between these parameters and the magnetopause size and shape are constructed by the Levenberg-Marquardt method for nonlinear multiparameter fitting step-by-step over the divided regions. It is noted that the asymmetries of the global structure of the magnetopause and the indentations near the cusps are described in this new model. The saturation influence of IMF B_z on the subsolar distance and the extrapolation of the tail magnetopause are also considered in this model. The main results are obtained as follows:

[43] 1. A new magnetopause model function has been developed on the basis of the Shue model function. It can appropriately describe a three-dimensional asymmetric magnetopause shape, including the asymmetries and the indentations.

[44] 2. A new continuous function is developed to describe the relationships between the IMF B_z and the magnetopause size and shape without using piecewise functions.

[45] 3. The new model is developed and parameterized by $P_d + P_m$, IMF B_z, and ϕ.

[46] 4. This new model improves the forecast accuracy and capability for the global near-Earth magnetopause, especially for the indentation regions.

[47] 5. The power law index for the subsolar distance versus $P_d + P_m$ is a bit less than −1/6, and the northward IMF B_z almost does not influence the magnetopause.

[48] 6. The magnetopause shape is asymmetric. The asymmetry along the Z direction is affected by the corrected dipole tilt angle, but it has little influence on the asymmetry along the Y direction. In cGSM coordinates, when ϕ = 0°, the asymmetry along the Y direction or along the Z direction is not obvious, whereas the size of the magnetopause along the Z direction is obviously less than that along the Y direction in the indentation regions.

[49] 7. There are indentations near the south and the north cups. Their location is mainly controlled by the corrected dipole tilt angle, and their depth is controlled by the solar wind dynamic and magnetic pressures.

[50] In this paper, we develop only an initial three-dimensional magnetopause model and briefly discuss the basic characteristics of this model. More work should be done to perfect the global magnetopause model. More comparisons of our model with previous models and the new model's ability to predict the near-Earth magnetopause under extreme solar wind conditions and for the distant tail magnetopause under various solar wind conditions also should be further investigated.

[51] **Acknowledgments.** We thank the National Aeronautics and Space Administration (NASA) for the satellite data and the Hawkeye magnetopause crossings' data, and we thank the Center for Space Science and Applied Research, Chinese Academy of Sciences, for the TC1 data. We are also grateful to S. A. Boardsen for providing the procedures for applying his model. This work was supported by grants from the Major State Basic Research Development Program of China (973 Program, G2006CB806300), the National Natural Science Foundation of China (40774079 and 40890160), the National High Technology Research and Development Program of China (863 Program, 2007AA12Z314), and the Special Fund for Public Welfare Industry (meteorology: GYHY200806024).

[52] Zuyin Pu thanks James Slavin and another reviewer for their assistance in evaluating this paper.

References

Boardsen, S. A., T. E. Eastman, T. Sotirelis, and J. L. Green (2000), An empirical model of the high-latitude magnetopause, *J. Geophys. Res.*, *105*(A10), 23,193–23,219, doi:10.1029/1998JA000143.

Chao, J. K., D. J. Wu, C.-H. Lin, Y. H. Yang, X. Y. Wang, M. Kessel, S. H. Chen, and R. P. Lepping (2002), Models for the size and shape of the Earth's magnetopause and bow shock, in *Space Weather Study Using Multipoint Techniques*, *COSPAR Colloq. Ser.*, vol. 12, edited by L.-H. Lyu, pp. 127–134, Pergamon, Oxford.

Eastman, T., S. A. Boardsen, S.-H. Chen, S. Fung, and R. Kessel (2000), Configuration of high-latitude and high-altitude boundary layers, *J. Geophys. Res.*, *105*(A10), 23,221–23,238, doi:10.1029/1999JA900269.

Fairfield, D. H. (1971), Average and unusual locations of the Earth's magnetopause and bow shock, *J. Geophys. Res.*, *76*(28), 6700–6716, doi:10.1029/JA076i028p06700.

Formisano, V., V. Domingo, and K.-P. Wenzel (1979), The three-dimensional shape of the magnetopause, *Planet. Space Sci.*, *27*, 1137–1149, doi:10.1016/0032-0633(79)90134-X.

Holzer, R. E., and J. A. Slavin (1978), Magnetic flux transfer associated with expansions and contractions of the dayside magnetosphere, *J. Geophys. Res.*, *83*(A8), 3831–3839, doi:10.1029/JA083iA08p03831.

Howe, H. C., Jr., and J. H. Binsack (1972), Explorer 33 and 35 plasma observations of magnetosheath flow, *J. Geophys. Res.*, *77*(19), 3334–3344, doi:10.1029/JA077i019p03334.

Kalegaev, V. V., and Y. G. Lyutov (2000), The solar wind control of the magnetopause, *Adv. Space Res.*, *25*(7–8), 1489–1492, doi:10.1016/S0273-1177(99)00660-2.

Kawano, H., S. M. Petrinec, C. T. Russell, and T. Higuchi (1999), Magnetopause shape determinations from measured position and estimated flaring angle, *J. Geophys. Res.*, *104*(A1), 247–261, doi:10.1029/98JA02479.

Kuznetsov, S. N., and A. V. Suvorova (1996), Solar wind control of the magnetopause shape and location, *Radiat. Meas.*, *26*(3), 413–415, doi:10.1016/1350-4487(96)00017-0.

Kuznetsov, S. N., and A. V. Suvorova (1998), An empirical model of the magnetopause for broad ranges of solar wind pressure and B_z IMF, in *Polar Cap Boundary Phenomena*, edited by J. Moen et al., pp. 51–61, Kluwer Acad., Norwell, Mass.

Petrinec, S. M., and C. T. Russell (1993), An empirical model of the size and shape of the near-Earth magnetotail, *Geophys. Res. Lett.*, *20*(23), 2695–2698, doi:10.1029/93GL02847.

Petrinec, S. M., and C. T. Russell (1996), Near-Earth magnetotail shape and size as determined from the magnetopause flaring angle, *J. Geophys. Res.*, *101*(A1), 137–152, doi:10.1029/95JA02834.

Petrinec, S. M., P. Song, and C. T. Russell (1991), Solar cycle variations in the size and shape of the magnetopause, *J. Geophys. Res.*, *96*(A5), 7893–7896, doi:10.1029/90JA02566.

Phan, T. D., et al. (1997), Low-latitude dusk flank magnetosheath, magnetopause, and boundary layer for low magnetic shear: Wind observations, *J. Geophys. Res.*, *102*(A9), 19,883–19,895, doi:10.1029/97JA01596.

Press, W. H., S. A. Teukolsky, W. T. Vetterling, and B. P. Flannery (1992), *Numerical Recipes in FORTRAN 77*, Cambridge Univ. Press, New York.

Roelof, E. C., and D. G. Sibeck (1993), Magnetopause shape as a bivariate function of interplanetary magnetic field B_z and solar wind dynamic pressure, *J. Geophys. Res.*, *98*(A12), 21,421–21,450, doi:10.1029/93JA02362.

Šafránková, J., Z. Němeček, Š. Dušík, L. Přech, D. G. Sibeck, and N. N. Borodkova (2002), The magnetopause shape and location: A comparison of the Interball and Geotail observations with models, *Ann. Geophys.*, *20*, 301–309.

Šafránková, J., Š. Dušík, and Z. Němeček (2005), The shape and location of the high-latitude magnetopause, *Adv. Space Res.*, *36*(10), 1934–1939, doi:10.1016/j.asr.2004.05.009.

Shue, J.-H., J. K. Chao, H. C. Fu, C. T. Russell, P. Song, K. K. Khurana, and H. J. Singer (1997), A new functional form to study the solar wind control of the magnetopause size and shape, *J. Geophys. Res.*, *102*(A5), 9497–9511, doi:10.1029/97JA00196.

Shue, J.-H., et al. (1998), Magnetopause location under extreme solar wind conditions, *J. Geophys. Res.*, *103*(A8), 17,691–17,700, doi:10.1029/98JA01103.

Shue, J.-H., P. Song, C. T. Russell, J. K. Chao, and Y.-H. Yang (2000), Toward predicting the position of the magnetopause within geosynchronous orbit, *J. Geophys. Res.*, *105*(A2), 2641–2656, doi:10.1029/1999JA900467.

Shue, J.-H., P. Song, C. T. Russell, M. F. Thomsen, and S. M. Petrinec (2001), Dependence of magnetopause erosion on southward interplanetary magnetic field, *J. Geophys. Res.*, *106*(A9), 18,777–18,788, doi:10.1029/2001JA900039.

Sibeck, D. G., R. E. Lopez, and E. C. Roelof (1991), Solar wind control of the magnetopause shape, location, and motion, *J. Geophys. Res.*, *96*(A4), 5489–5495, doi:10.1029/90JA02464.

Slavin, J. A., E. J. Smith, D. G. Sibeck, D. N. Baker, R. D. Zwickl, and S.-I. Akasofu (1985), An ISEE 3 study of average and substorm conditions in the distant magnetotail, *J. Geophys. Res.*, *90*(A11), 10,875–10,895, doi:10.1029/JA090iA11p10875.

Spreiter, J. R., A. L. Summers, and A. Y. Alksne (1966), Hydromagnetic flow around the magnetosphere, *Planet. Space Sci.*, *14*, 223–253, doi:10.1016/0032-0633(66)90124-3.

Tsyganenko, N. A. (1996), Effects of the solar wind conditions on the global magnetospheric configuration as deduced from data-based field models, *Eur. Space Agency Spec. Publ.*, *ESA SP-89*, 181.

Yang, Y.-H., J. K. Chao, C.-H. Lin, J.-H. Shue, X.-Y. Wang, P. Song, C. T. Russell, R. P. Lepping, and A. J. Lazarus (2002), Comparison of three magnetopause prediction models under extreme solar wind conditions, *J. Geophys. Res.*, *107*(A1), 1008, doi:10.1029/2001JA000079.

Yang, Y.-H., J. K. Chao, A. V. Dmitriev, C.-H. Lin, and D. M. Ober (2003), Saturation of IMF B_z influence on the position of dayside magnetopause, *J. Geophys. Res.*, *108*(A3), 1104, doi:10.1029/2002JA009621.

Zhou, X.-W., and C. T. Russell (1997), The location of the high-latitude polar cusp and the shape of the surrounding magnetopause, *J. Geophys. Res.*, *102*(A1), 105–110, doi:10.1029/96JA02702.

Zhou, X. W., C. T. Russell, G. Le, S. A. Fuselier, and J. D. Scudder (2000), Solar wind control of the polar cusp at high altitude, *J. Geophys. Res.*, *105*(A1), 245–251, doi:10.1029/1999JA900412.

J. C. Gong, R. L. Lin, and S. Q. Liu, Center for Space Science and Applied Research, Chinese Academy of Sciences, Beijing 100190, China. (rllin04@163.com)

Y. L. Wang, NASA Goddard Space Flight Center, Greenbelt, MD 20771-0003, USA.

X. X. Zhang (corresponding author), National Center for Space Weather, China Meteorological Administration, Beijing 100081, China.